

## Supporting Information

### Double-Crack Structure for Bionic Wearable Strain Sensor with Ultra-high Sensitivity and Wide Sensing Range

Di Zhu, <sup>#a</sup> Shengshun Duan, <sup>#a</sup> Jiachen Liu, <sup>a</sup> Shanyan Diao, <sup>a</sup> Jianlong Hong, <sup>a</sup> Shengxin Xiang, <sup>a</sup> Xiao Wei, <sup>a</sup> Peng Xiao, <sup>b</sup> Jun Xia, <sup>a</sup> Wei Lei, <sup>a</sup> Baoping Wang, <sup>a</sup> Qiongfeng Shi<sup>a</sup> and Jun Wu<sup>\*a</sup>

<sup>a</sup>Joint International Research Laboratory of Information Display and Visualization, School of Electronic Science and Engineering, Southeast University, 210096, China

E-mail: [wujunseu@seu.edu.cn](mailto:wujunseu@seu.edu.cn)

<sup>b</sup>State Grid Jiangsu Electric Power Co., Ltd. Research Institute, Nanjing, 211103, Jiangsu, P. R. China

Email: [vodoco@foxmail.com](mailto:vodoco@foxmail.com)

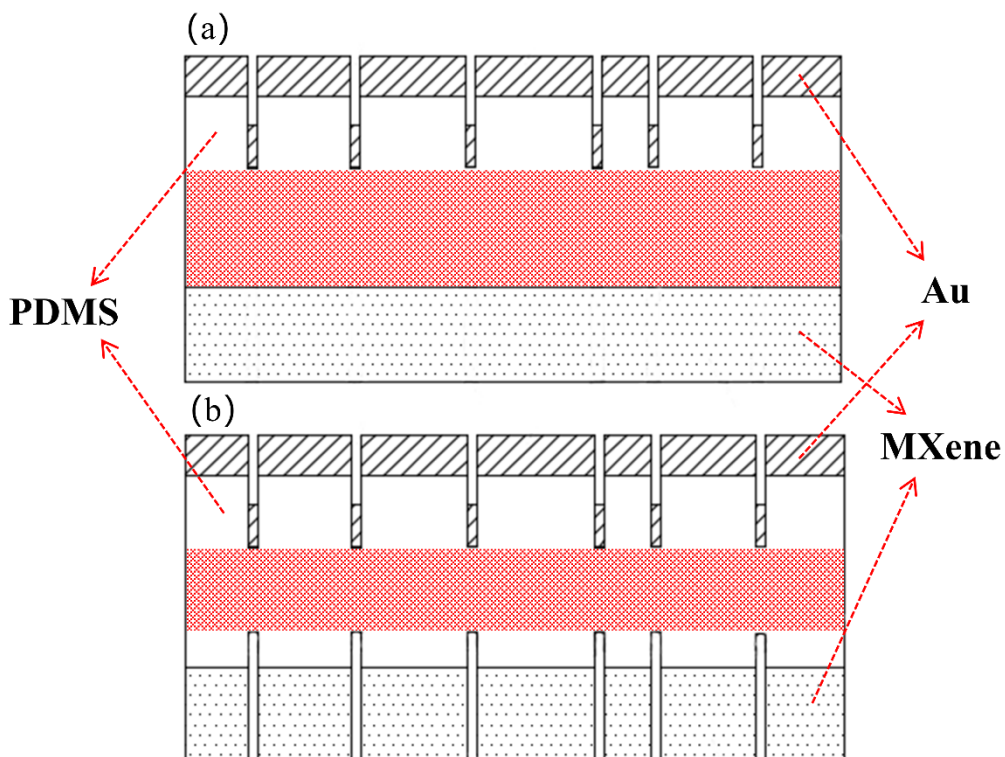


**Fig. S1** Sectional view of the flexible strain sensor (a) without and (b) with cracks on the MXene layer.

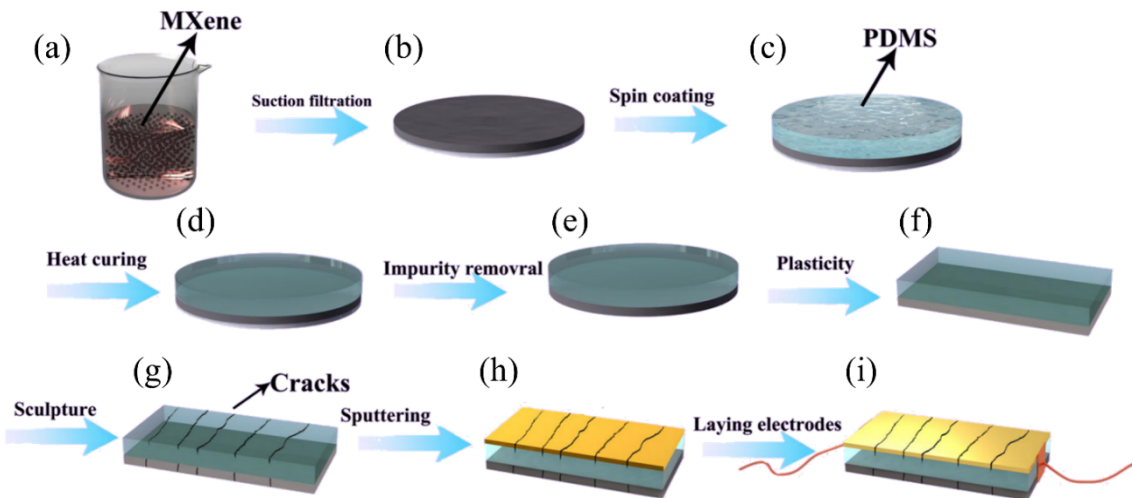


**Fig. S2** The fabrication approach of the flexible strain sensor. (a) The MXene aqueous dispersion. (b) The filter membrane with a pore size of 220 nm could be used for suction filtration to obtain the filter membrane with MXene sheets. (c) The mixed PDMS was spin-coated on the MXene sheets by using a spin coater. (d) After heat curing, the liquid PDMS on the surface became a solid PDMS film. (e) The filter membrane could be easily peeled off to obtain PMCs. (f) The PMCs were cut into a 3.0 cm×1.0 cm×0.1 cm cuboid. (g) The cracks were carved on both sides of the PMCs by an engraving machine. (h) The Au film was formed on the PDMS through the vacuum evaporation technique. (i) The two wires were attached on the two sides of the sensors by the copper foil and silver paste, where the copper foil is used to conductively connect the upper Au film and the bottom MXene layer.

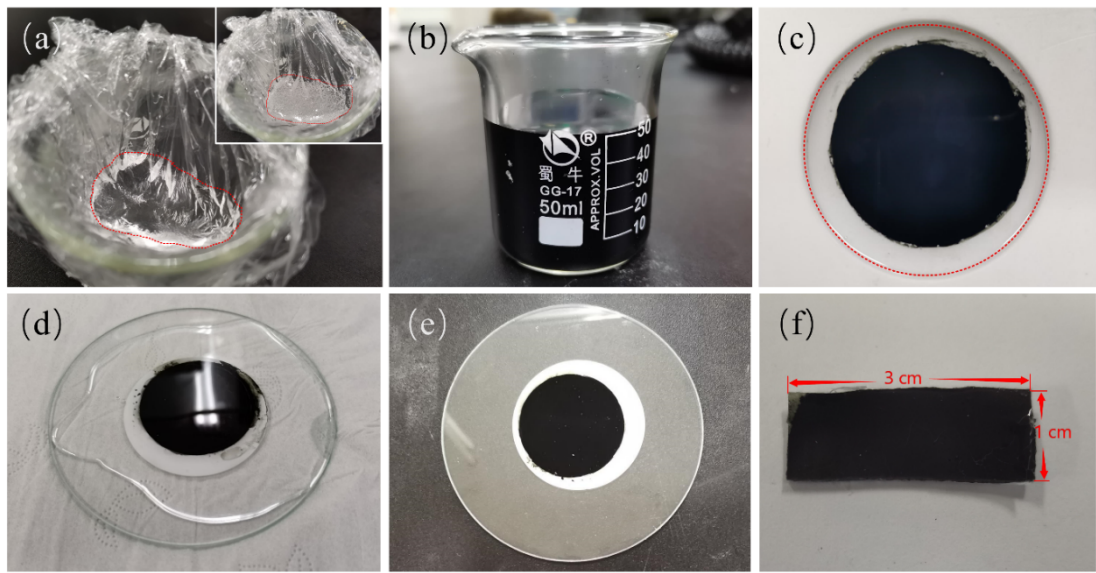


**Fig. S3** Some physical photos of the preparation of PMCs. (a) Changes of PDMS before and after vacuum. (b) Diluted MXene aqueous dispersion. (c) Filter paper with MXene sheets attached. (d) PDMS before curing. (e) PDMS membrane containing MXene and filter membrane after curing. (f) Schematic diagram of rectangular PMCs and dimensions.

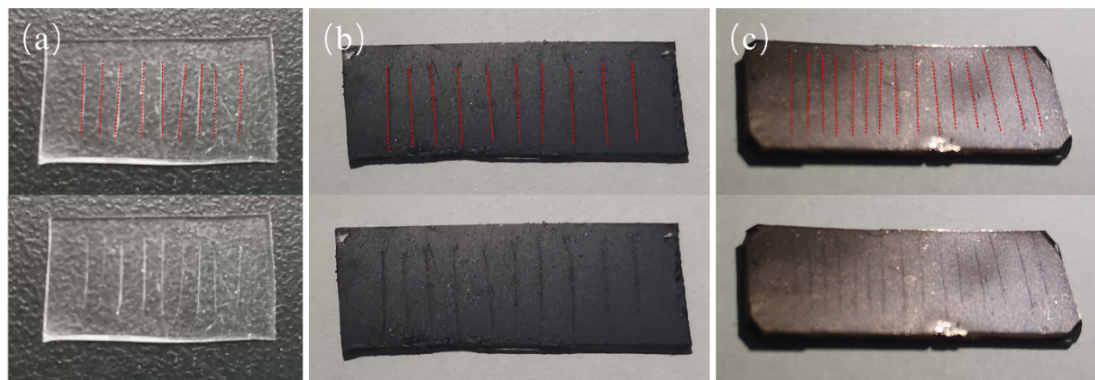


**Fig. S4** Physical photos of cracks carved on different material surfaces. (a) Engraved cracks on the PDMS layer. (b) Engraved cracks on the MXene layer. (c) The metal layer on the PDMS layer engraved with cracks also has a crack structure.

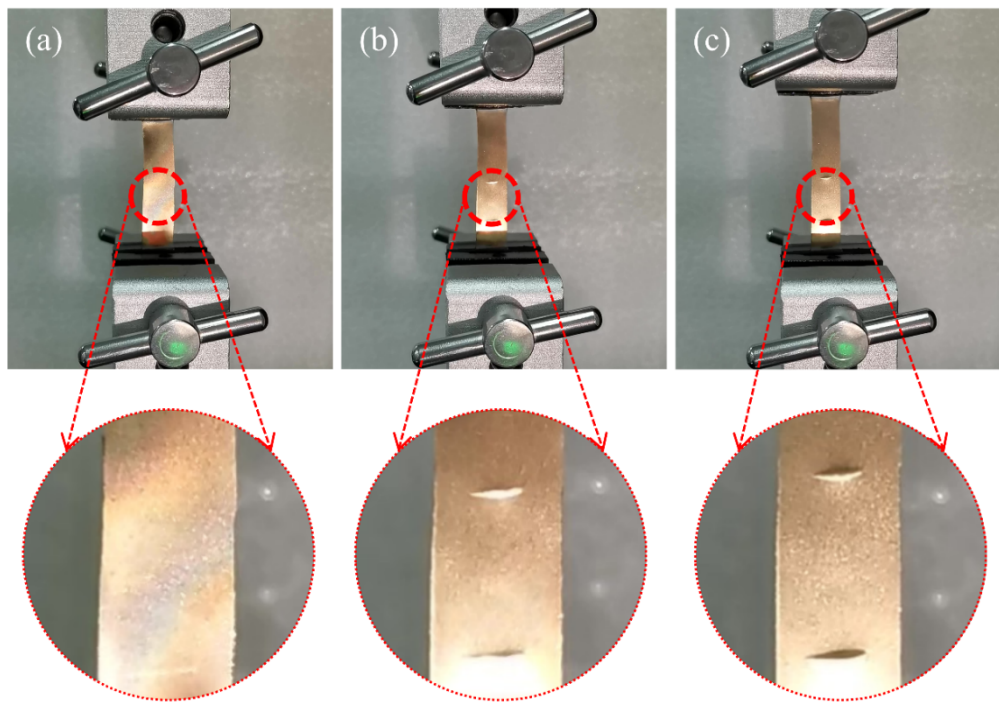


**Fig. S5** Photographs of cracks on the Au layer opening under tension.

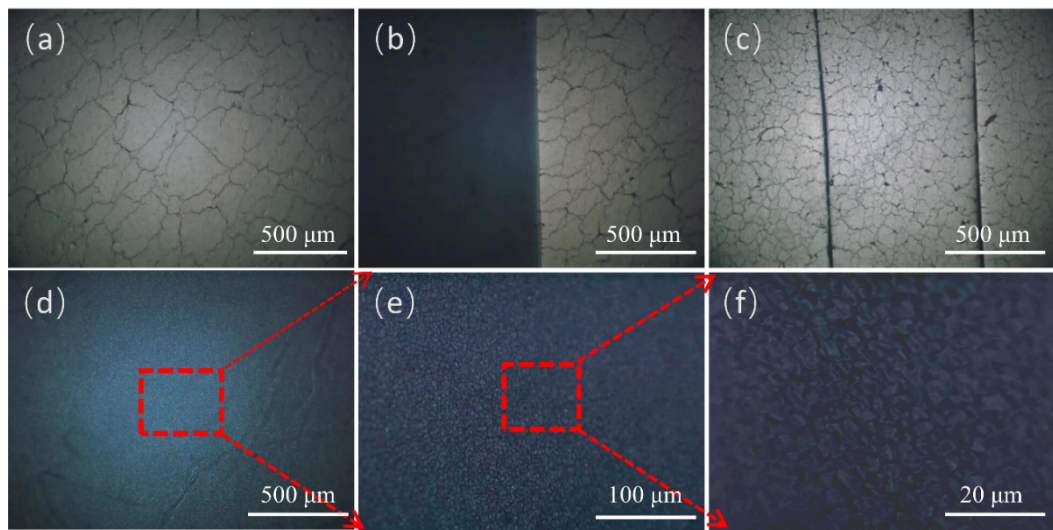


**Fig. S6** The micro-structure of the APMCs observed by a high-speed digital microscope. (a) The Au layer. (b) The contact surface between PDMS and Au layer. (c) Cracks on the Au layer. (d-f) The surface of the MXene layer at different magnifications.

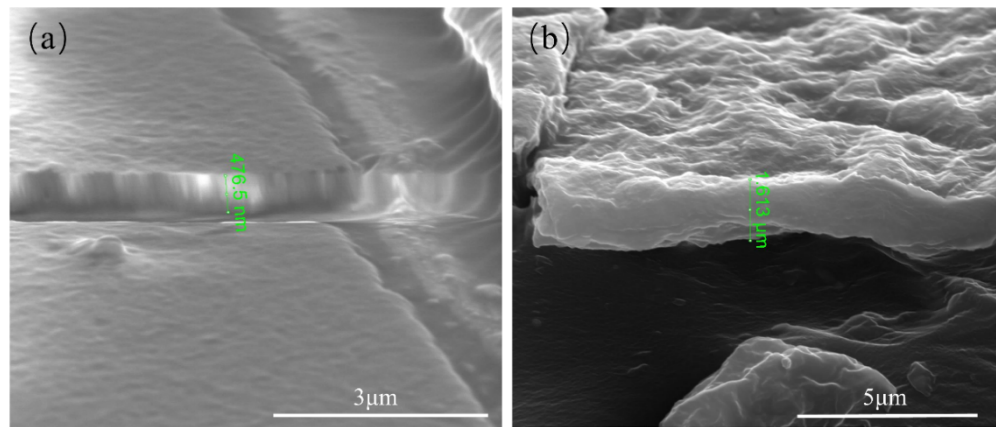


**Fig. S7** SEM images of the profiles of (a) the Au layer and (b) the MXene layer.

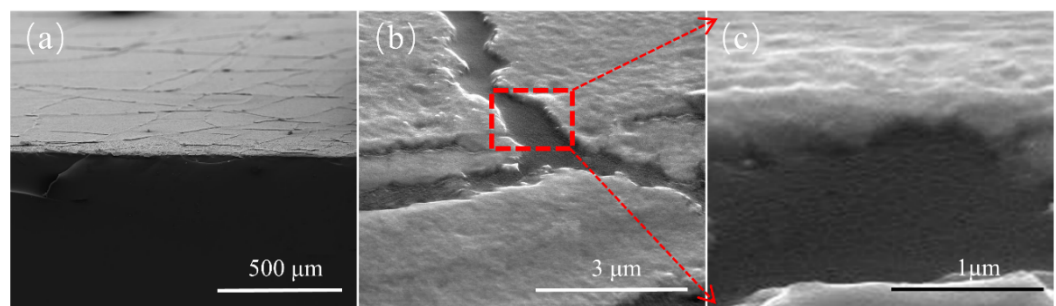


**Fig. S8** SEM images of (a) the contact surface between the Au layer and the PDMS layer, and (b-c) the nano-scale cracks on the Au layer.

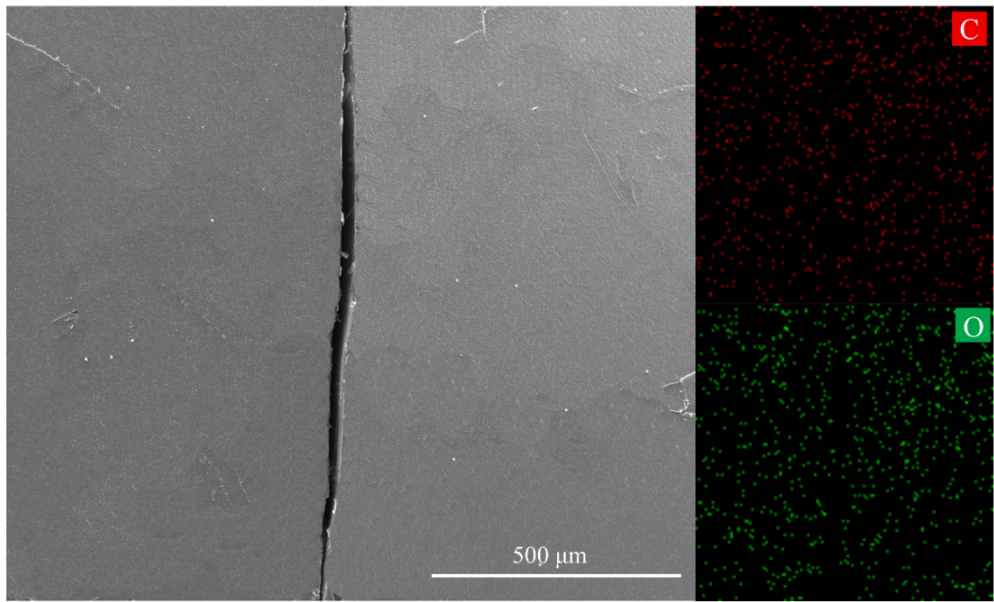


**Fig. S9** EDS mapping images of a micron-scale crack on the MXene layer showed the distribution of C and O elements.

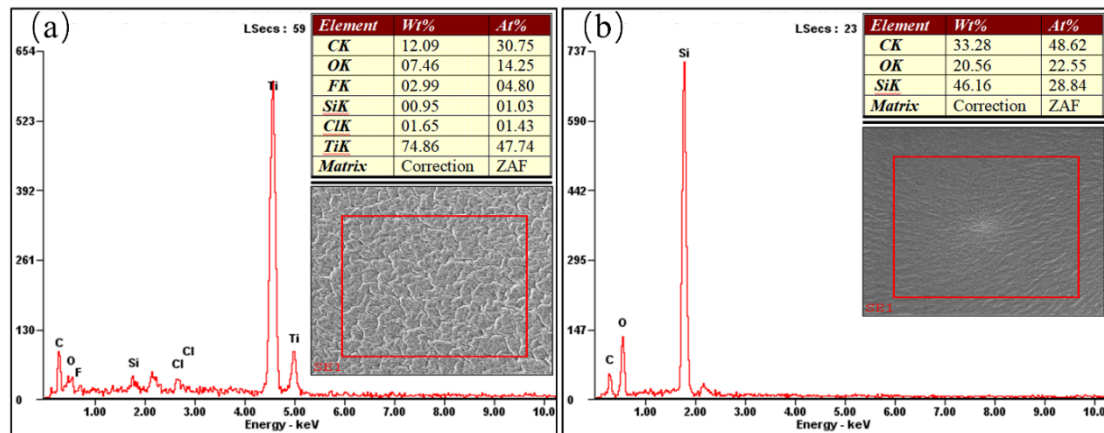


**Fig. S10** EDS images of (a) the MXene layer and (b) the PDMS layer measured by an energy-dispersive X-ray spectroscopic detector.

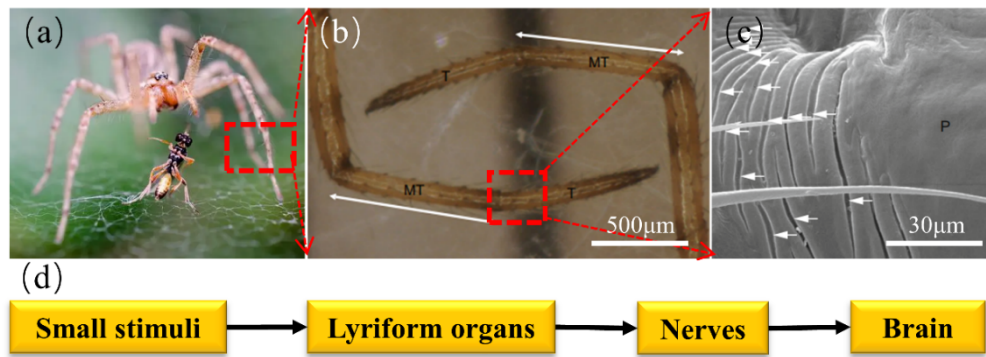


**Fig. S11** Bionics basis of the strain sensor based on cracks<sup>1</sup>. (a) Arthropods such as spiders. (b) The lower foot joints of spiders. (c) An SEM image of the lyriform organs. (d) The transmission flowchart of information.

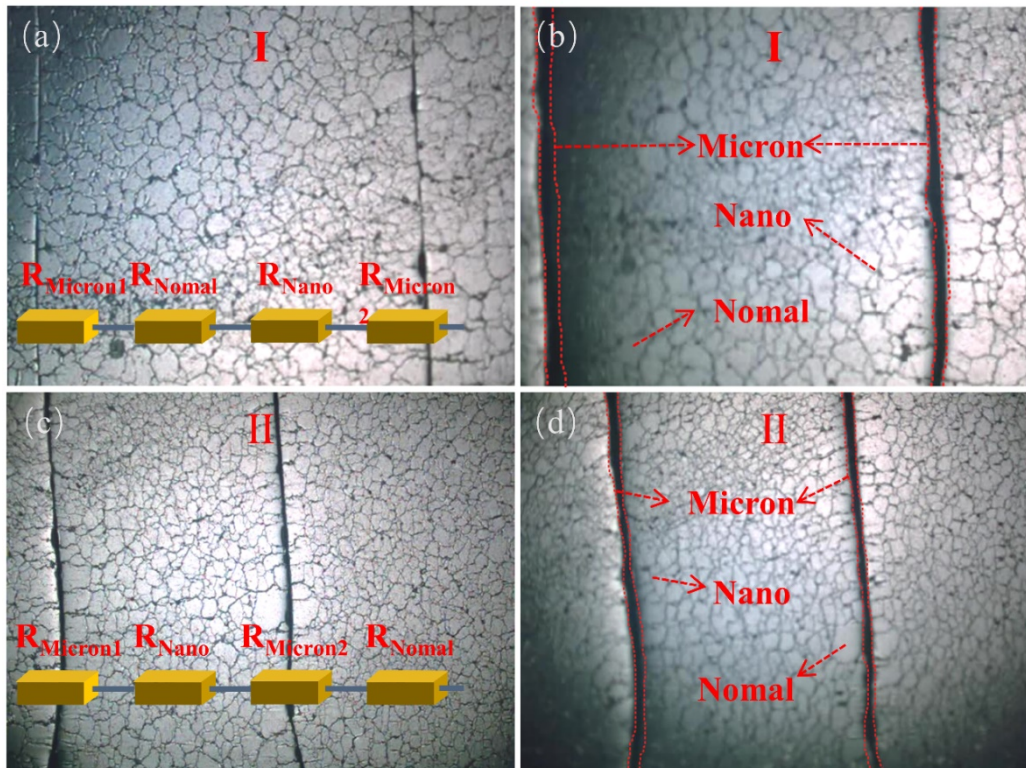


**Fig. S12** The changes in the cracks on the Au layer before and after opening were observed by a high-speed digital microscope. (a-b) Equivalent series resistance in zone I. (c-d) Equivalent series resistance in zone II.

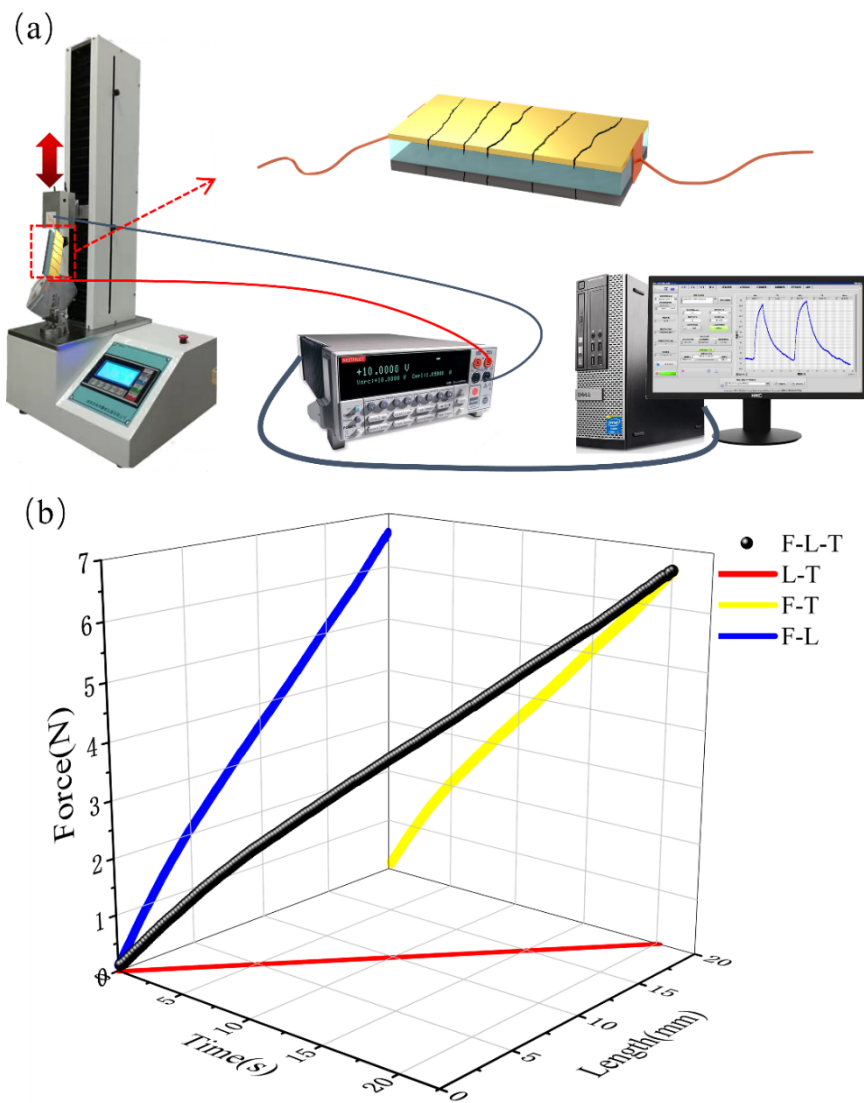


**Fig. S13** (a) Deformation sensing performance testing system. (b) The relationship between time, tensile length, and tensile force in a tensile test.

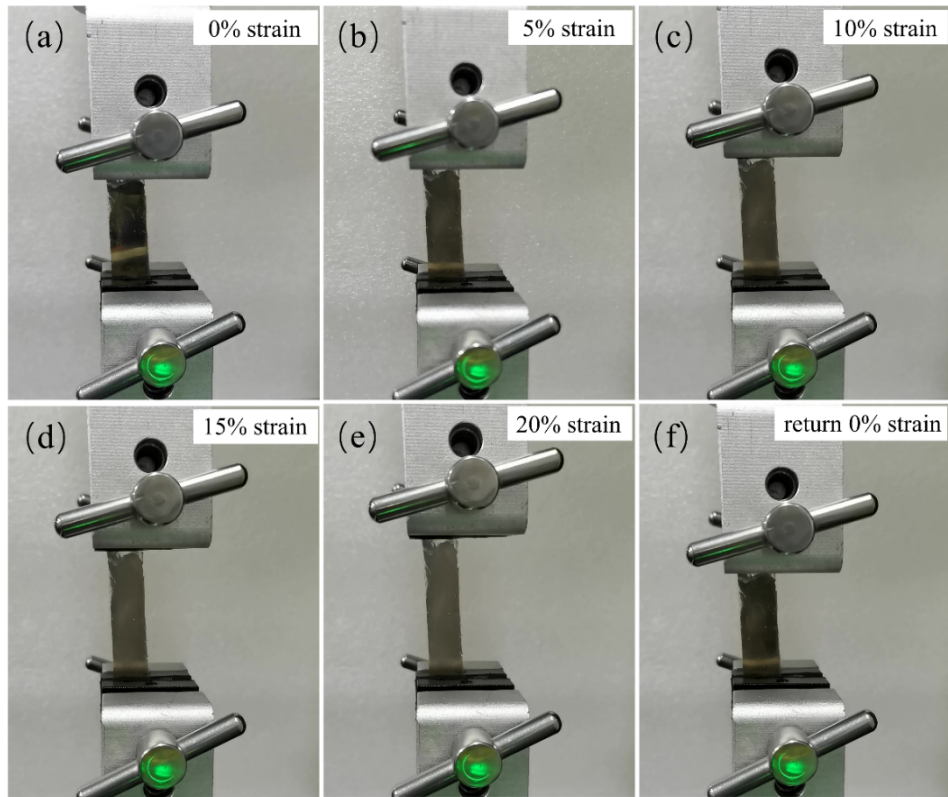


**Fig. S14** State and recovery stability of the APMCs under (a) 0% strain, (b) 5% strain, (c) 10% strain, (d) 15% strain, (e) 20% strain, and (f) returning 0% strain.

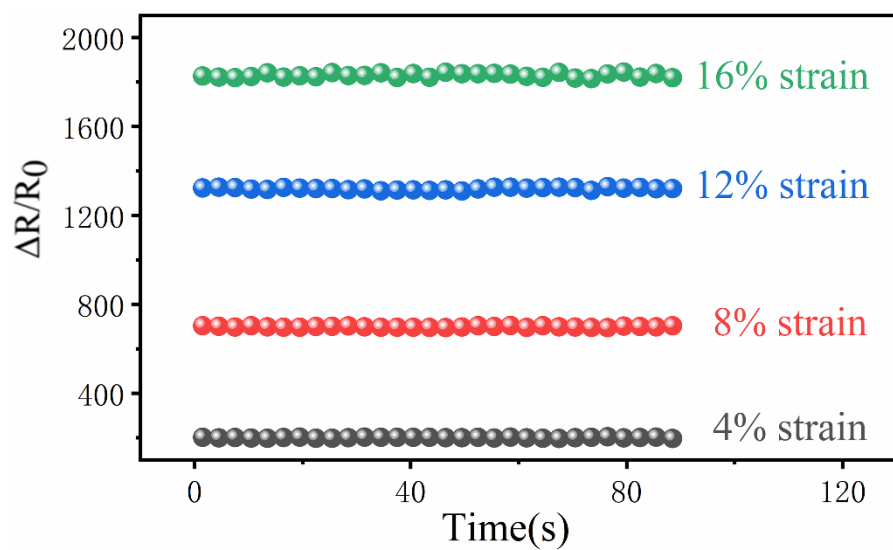


**Fig. S15** Stability of the strain sensor's resistance variation under different strains.

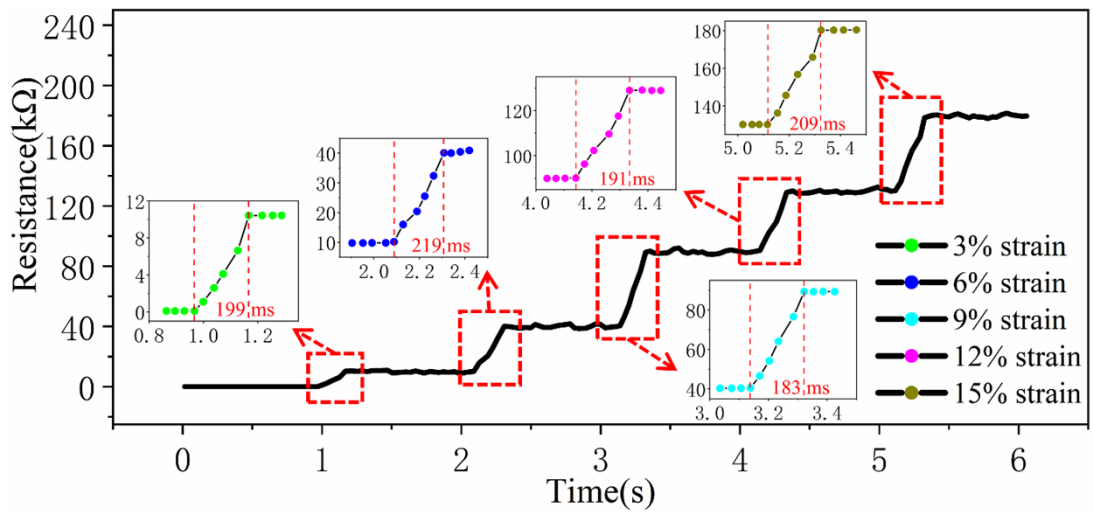


**Fig. S16** Response time curve of device resistance change under different deformations and distribution of five resistance response regions.

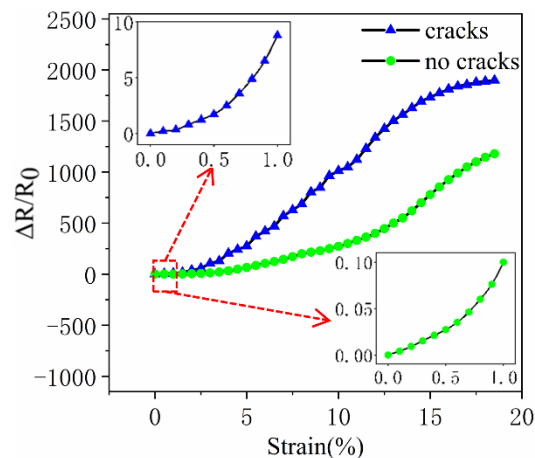
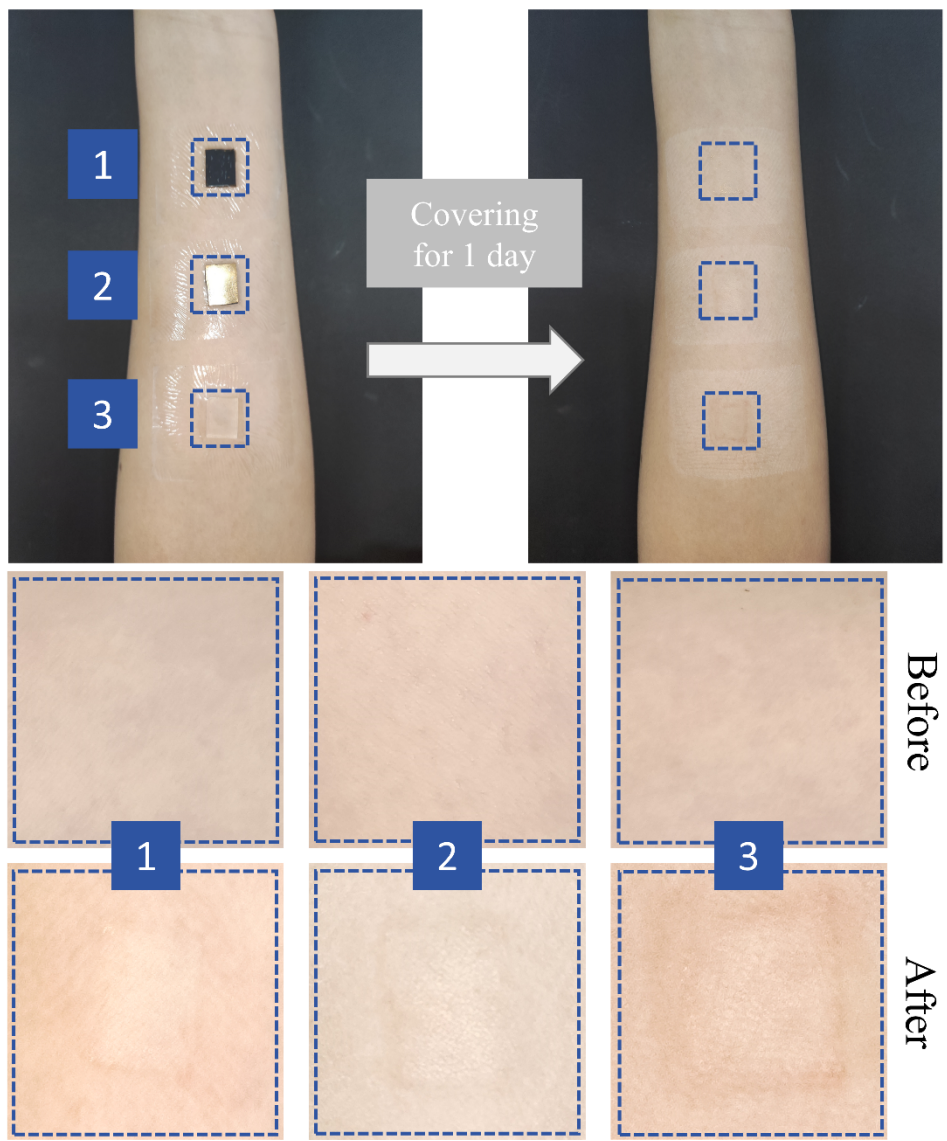


**Fig. S17** Resistance variation-strain curves of strain sensors with cracks and without cracks respectively within working range. Insets, result for sensing performance of two devices under 0-1% strain.



1: Au layer contact; 2: MXene layer contact; 3: PDMS film contact

**Fig. S18** Digital images showing the skin irritation results of different materials on the forearms of the volunteer.

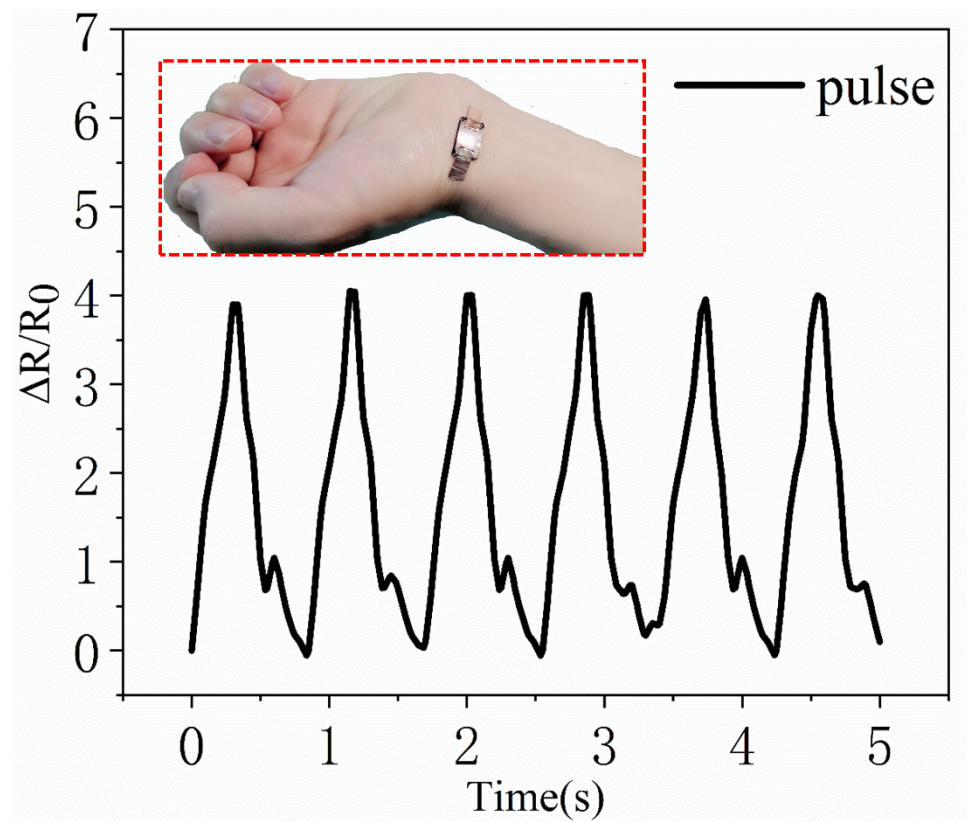


**Fig. S19** The sensor's resistance response to pulse was monitored.

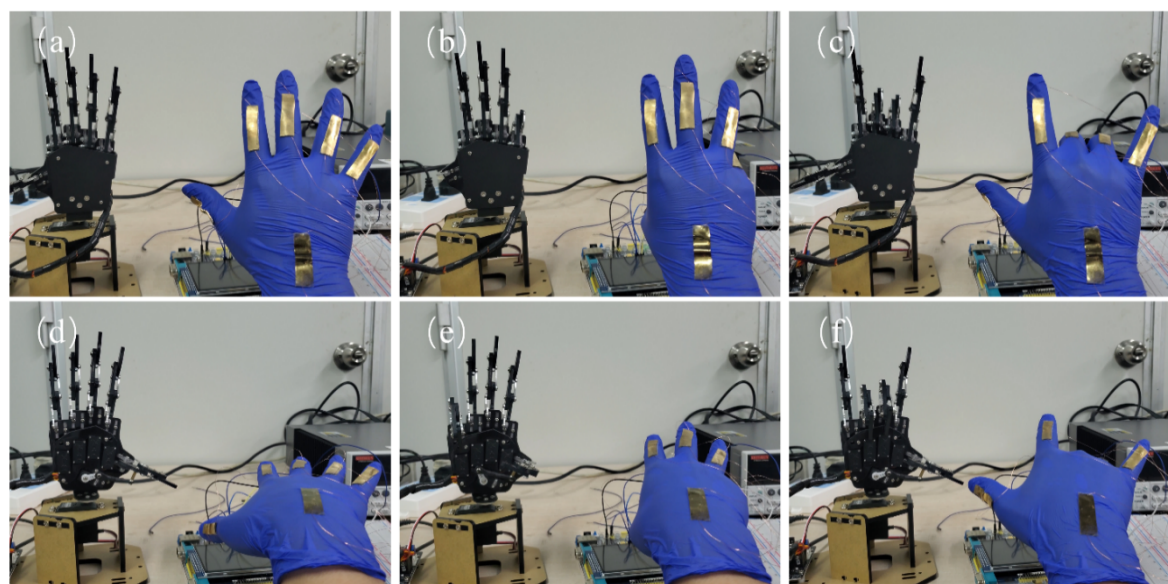


**Fig. S20** Gesture screenshot of a sensing glove based on APMCs controlling machine hand.

**Video S1.** Stretching of APMCs.

**Video S2.** Control robots for human-machine interaction.

## References

- 1 E. L. Morley, S. Sivalinghem, A. C. Mason, *Zoomorphology* 2016, 135, 433.